ACCEPTED BY THE ASTROPHYSICAL JOURNAL
Preprint typeset using LaTeX style emulateapj v. 5/2/11

arXiv:1411.4915v2 [astro-ph.HE] 13 Jan 2015

GAMMA-RAY FLARING ACTIVITY FROM THE GRAVITATIONALLY LENSED BLAZAR PKS 1830-211 OBSERVED BY *FERMI* LAT

A. A. ABDO[1], M. ACKERMANN[2], M. AJELLO[3], A. ALLAFORT[4], M. A. AMIN[5,62], L. BALDINI[6], G. BARBIELLINI[7,8], D. BASTIERI[9,10], K. BECHTOL[4], R. BELLAZZINI[6], R. D. BLANDFORD[4], E. BONAMENTE[11,12], A. W. BORGLAND[4], J. BREGEON[13], M. BRIGIDA[14,15], R. BUEHLER[2], D. BULMASH[16,62], S. BUSON[9,10,*], G. A. CALIANDRO[4,18], R. A. CAMERON[4], P. A. CARAVEO[19], E. CAVAZZUTI[20], C. CECCHI[11,12], E. CHARLES[4], C. C. CHEUNG[21], J. CHIANG[4], G. CHIARO[10], S. CIPRINI[20,22,*], R. CLAUS[4], J. COHEN-TANUGI[13], J. CONRAD[23,24,25,26], R. H. D. CORBET[27,28], S. CUTINI[20,22], F. D'AMMANDO[29,*], A. DE ANGELIS[30], F. DE PALMA[14,15], C. D. DERMER[21], P. S. DRELL[4], A. DRLICA-WAGNER[31], C. FAVUZZI[14,15], J. FINKE[21,*], W. B. FOCKE[4], Y. FUKAZAWA[32], P. FUSCO[14,15], F. GARGANO[15], D. GASPARRINI[20,22], N. GEHRELS[33], N. GIGLIETTO[14,15], F. GIORDANO[14,15], M. GIROLETTI[29], T. GLANZMAN[4], I. A. GRENIER[34], J. E. GROVE[21], S. GUIRIEC[33,35], D. HADASCH[36], M. HAYASHIDA[37], E. HAYS[33], R. E. HUGHES[38], Y. INOUE[4], M. S. JACKSON[39,24], T. JOGLER[4], G. JÓHANNESSON[40], A. S. JOHNSON[4], T. KAMAE[4], J. KNÖDLSEDER[41,42], M. KUSS[6], J. LANDE[4], S. LARSSON[23,24,43], L. LATRONICO[44], F. LONGO[7,8], F. LOPARCO[14,15], B. LOTT[45], M. N. LOVELLETTE[21], P. LUBRANO[11,12], G. M. MADEJSKI[4], M. N. MAZZIOTTA[15], J. MEHAULT[45], P. F. MICHELSON[4], T. MIZUNO[46], M. E. MONZANI[4], A. MORSELLI[47], I. V. MOSKALENKO[4], S. MURGIA[48], R. NEMMEN[33,27,28], E. NUSS[13], M. OHNO[32], T. OHSUGI[46], D. PANEQUE[49,4], J. S. PERKINS[33], M. PESCE-ROLLINS[6], F. PIRON[13], G. PIVATO[10], T. A. PORTER[4], S. RAINÒ[14,15], R. RANDO[9,10], M. RAZZANO[6,50], A. REIMER[36,4], O. REIMER[36,4], L. C. REYES[51], S. RITZ[52], C. ROMOLI[10], M. ROTH[53], P. M. SAZ PARKINSON[52,54], C. SGRÒ[6], E. J. SISKIND[55], G. SPANDRE[6], P. SPINELLI[14,15], H. TAKAHASHI[32], Y. TAKEUCHI[56], T. TANAKA[57], J. G. THAYER[4], J. B. THAYER[4], D. J. THOMPSON[33], L. TIBALDO[4], M. TINIVELLA[6], D. F. TORRES[58,59], G. TOSTI[11,12], E. TROJA[33,60], V. TRONCONI[10], T. L. USHER[4], J. VANDENBROUCKE[4], V. VASILEIOU[13], G. VIANELLO[4], V. VITALE[47,61], A. P. WAITE[4], M. WERNER[36], B. L. WINER[38], K. S. WOOD[21]

Accepted by The Astrophysical Journal

ABSTRACT

The Large Area Telescope (LAT) on board the *Fermi* Gamma-ray Space Telescope routinely detects the MeV-peaked flat spectrum radio quasar PKS 1830−211 ($z = 2.507$). Its apparent isotropic γ-ray luminosity ($E > 100$ MeV) averaged over ~ 3 years of observations and peaking on 2010 October 14/15 at 2.9×10^{50} erg s^{-1}, makes it among the brightest high-redshift *Fermi* blazars. No published model with a single lens can account for all of the observed characteristics of this complex system. Based on radio observations, one expects time delayed variability to follow about 25 days after a primary flare, with flux about a factor 1.5 less. Two large γ-ray flares of PKS 1830−211 have been detected by the LAT in the considered period and no substantial evidence for such a delayed activity was found. This allows us to place a lower limit of about 6 on the γ rays flux ratio between the two lensed images. *Swift* XRT observations from a dedicated Target of Opportunity program indicate a hard spectrum and with no significant correlation of X-ray flux with the γ-ray variability. The spectral energy distribution can be modeled with inverse Compton scattering of thermal photons from the dusty torus. The implications of the LAT data in terms of variability, the lack of evident delayed flare events, and different radio and γ-ray flux ratios are discussed. Microlensing effects, absorption, size and location of the emitting regions, the complex mass distribution of the system, an energy-dependent inner structure of the source, and flux suppression by the lens galaxy for one image path may be considered as hypotheses for understanding our results.

Subject headings: gamma rays: galaxies – gamma rays: general – gravitational lensing: strong – quasars: individual: (PKS 1830-211) – X-rays: individual (PKS 1830-211) – radiation mechanisms: nonthermal

* Corresponding authors:
S. Ciprini, stefano.ciprini@asdc.asi.it, S. Buson, sara.buson@pd.infn.it, J. Finke, justin.finke@nrl.navy.mil, F. D'Ammando, dammando@ira.inaf.it

[1] Center for Earth Observing and Space Research, College of Science, George Mason University, Fairfax, VA 22030, resident at Naval Research Laboratory, Washington, DC 20375, USA

[2] Deutsches Elektronen Synchrotron DESY, D-15738 Zeuthen, Germany

[3] Space Sciences Laboratory, 7 Gauss Way, University of California, Berkeley, CA 94720-7450, USA

[4] W. W. Hansen Experimental Physics Laboratory, Kavli Institute for Particle Astrophysics and Cosmology, Department of Physics and SLAC National Accelerator Laboratory, Stanford University, Stanford, CA 94305, USA

[5] Kavli Institute for Cosmology and Institute of Astronomy, University of Cambridge, Madingley Road, Cambridge CB3 0HA, UK,

[6] Istituto Nazionale di Fisica Nucleare, Sezione di Pisa, I-56127 Pisa, Italy

[7] Istituto Nazionale di Fisica Nucleare, Sezione di Trieste, I-34127 Trieste, Italy

[8] Dipartimento di Fisica, Università di Trieste, I-34127 Trieste, Italy

[9] Istituto Nazionale di Fisica Nucleare, Sezione di Padova, I-35131 Padova, Italy

[10] Dipartimento di Fisica e Astronomia "G. Galilei", Università di Padova, I-35131 Padova, Italy

[11] Istituto Nazionale di Fisica Nucleare, Sezione di Perugia, I-06123 Perugia, Italy

[12] Dipartimento di Fisica, Università degli Studi di Perugia, I-06123 Perugia, Italy

[13] Laboratoire Univers et Particules de Montpellier, Université Montpellier 2, CNRS/IN2P3, Montpellier, France

[14] Dipartimento di Fisica "M. Merlin" dell'Università e del Politecnico di Bari, I-70126 Bari, Italy

[15] Istituto Nazionale di Fisica Nucleare, Sezione di Bari, 70126 Bari, Italy

[16] Department of Physics, Stanford University, Stanford, CA 94305, USA

[18] Consorzio Interuniversitario per la Fisica Spaziale (CIFS), I-10133 Torino, Italy

[19] INAF-Istituto di Astrofisica Spaziale e Fisica Cosmica, I-20133 Milano, Italy

1. INTRODUCTION

The flat spectrum radio quasar (FSRQ) PKS 1830−211 (also known as TXS 1830−210, RX J1833.6−210, MRC 1830−211, 2FGL J1833.6−2104) has met with considerable attention, because it is such a good example of a gravitationally lensed source. The two lines of sight towards PKS 1830−211 have been used as a cosmological probe: temperature of the cosmic microwave background, variations in the fundamental constants, the Hubble constant estimation (Bagdonaite et al. 2013; Blandford & Narayan 1992). This object also offers a unique opportunity to study both the interstellar medium of lens galaxy and the relativistic jet of the background γ-ray blazar. PKS 1830−211 was discovered as a single source in the Parkes catalog, but later radio observations by the Very Large Array (VLA) and Australian Telescope Compact Array (ATCA) clearly revealed two sources, one in the northeast (NE) and one in the southwest (SW), separated by $0.98''$ and connected by an Einstein ring (Pramesh Rao & Subrahmanyan 1988; Jauncey et al. 1991). When the source, lensing foreground object, and observer lie along a straight line, the theory of gravitational lensing (e.g. Einstein 1936) shows that a circle, known as the Einstein ring, may be formed (Schneider et al. 1992), while smaller rings could appear inside this main ring if the lens is a Schwarzschild black hole. The lens magnification factor is the ratio of the flux of the lens image to the flux of the unlensed source, and is equal to the ratio of the solid angles of the image, and the unlensed source. The NE image has a radio flux density about 1.5 times as bright as the SW one at 8.6 GHz (Lovell et al. 1998). Molecular absorption lines revealed lensing galaxies located at $z = 0.88582$ (Wiklind & Combes 1996; Lovell et al. 1996; Frye et al. 1999; Lehár et al. 2000; Muller et al. 2011; Aller et al. 2012) and $z = 0.19$ (Lovell et al. 1996) suggesting that PKS 1830−211 may be a compound gravitationally lensed system (Lovell et al. 1996). These lensing galaxies were confirmed by Gemini and *Hubble Space Telescope* (*HST*) (Courbin et al. 2002). A detailed exploration of this system at optical wavelengths is hampered by its proximity on the sky to the Galactic plane and the bulge of the Milky Way (the Galactic coordinates of PKS 1830−211 being $l = 12.17°$, $b = -5.71°$), leading to considerable dust extinction (Courbin et al. 1998; Gregg et al. 2002, and references therein) and absorption. Absorption by molecular species (> 30 different species) from the two foreground galaxies also peculiarly characterize the radio PKS 1830−211 (Wiklind & Combes 1996, 1998; Muller et al. 2011). Molecular absorptions from the intervening galaxy at $z = 0.886$, also allowed to put a limit on proton-to-electron mass ratio (Bagdonaite et al. 2013).

Despite its position near the Galactic plane and center, progress has been made in studying the source in the optical and near infrared (IR). Courbin et al. (1998, 2002) and Frye et al. (1999) used a deconvolution algorithm to create optical/near-IR images of the region, and found the counterparts to the radio sources, including highly reddened images

[20] Agenzia Spaziale Italiana (ASI) Science Data Center, I-00133 Roma, Italy
[21] Space Science Division, Naval Research Laboratory, Washington, DC 20375-5352, USA
[22] Istituto Nazionale di Astrofisica - Osservatorio Astronomico di Roma, I-00040 Monte Porzio Catone (Roma), Italy
[23] Department of Physics, Stockholm University, AlbaNova, SE-106 91 Stockholm, Sweden
[24] The Oskar Klein Centre for Cosmoparticle Physics, AlbaNova, SE-106 91 Stockholm, Sweden
[25] Royal Swedish Academy of Sciences Research Fellow, funded by a grant from the K. A. Wallenberg Foundation
[26] The Royal Swedish Academy of Sciences, Box 50005, SE-104 05 Stockholm, Sweden
[27] Center for Research and Exploration in Space Science and Technology (CRESST) and NASA Goddard Space Flight Center, Greenbelt, MD 20771, USA
[28] Department of Physics and Center for Space Sciences and Technology, University of Maryland Baltimore County, Baltimore, MD 21250, USA
[29] INAF Istituto di Radioastronomia, 40129 Bologna, Italy
[30] Dipartimento di Fisica, Università di Udine and Istituto Nazionale di Fisica Nucleare, Sezione di Trieste, Gruppo Collegato di Udine, I-33100 Udine, Italy
[31] Fermilab, Batavia, IL 60510, USA
[32] Department of Physical Sciences, Hiroshima University, Higashi-Hiroshima, Hiroshima 739-8526, Japan
[33] NASA Goddard Space Flight Center, Greenbelt, MD 20771, USA
[34] Laboratoire AIM, CEA-IRFU/CNRS/Université Paris Diderot, Service d'Astrophysique, CEA Saclay, 91191 Gif sur Yvette, France
[35] NASA Postdoctoral Program Fellow, USA
[36] Institut für Astro- und Teilchenphysik and Institut für Theoretische Physik, Leopold-Franzens-Universität Innsbruck, A-6020 Innsbruck, Austria
[37] Institute for Cosmic-Ray Research, University of Tokyo, 5-1-5 Kashiwanoha, Kashiwa, Chiba, 277-8582, Japan
[38] Department of Physics, Center for Cosmology and Astro-Particle Physics, The Ohio State University, Columbus, OH 43210, USA
[39] Department of Physics, KTH Royal Institute of Technology, AlbaNova, SE-106 91 Stockholm, Sweden
[40] Science Institute, University of Iceland, IS-107 Reykjavik, Iceland
[41] CNRS, IRAP, F-31028 Toulouse cedex 4, France
[42] GAHEC, Université de Toulouse, UPS-OMP, IRAP, Toulouse, France
[43] Department of Astronomy, Stockholm University, SE-106 91 Stockholm, Sweden
[44] Istituto Nazionale di Fisica Nucleare, Sezione di Torino, I-10125 Torino, Italy
[45] Centre d'Études Nucléaires de Bordeaux Gradignan, IN2P3/CNRS, Université Bordeaux 1, BP120, F-33175 Gradignan Cedex, France
[46] Hiroshima Astrophysical Science Center, Hiroshima University, Higashi-Hiroshima, Hiroshima 739-8526, Japan
[47] Istituto Nazionale di Fisica Nucleare, Sezione di Roma "Tor Vergata", I-00133 Roma, Italy
[48] Center for Cosmology, Physics and Astronomy Department, University of California, Irvine, CA 92697-2575, USA
[49] Max-Planck-Institut für Physik, D-80805 München, Germany
[50] Funded by contract FIRB-2012-RBFR12PM1F from the Italian Ministry of Education, University and Research (MIUR)
[51] Department of Physics, California Polytechnic State University, San Luis Obispo, CA 93401, USA
[52] Santa Cruz Institute for Particle Physics, Department of Physics and Department of Astronomy and Astrophysics, University of California at Santa Cruz, Santa Cruz, CA 95064, USA
[53] Department of Physics, University of Washington, Seattle, WA 98195-1560, USA
[54] Department of Physics, The University of Hong Kong, Pokfulam Road, Hong Kong, China
[55] NYCB Real-Time Computing Inc., Lattingtown, NY 11560-1025, USA
[56] Research Institute for Science and Engineering, Waseda University, 3-4-1, Okubo, Shinjuku, Tokyo 169-8555, Japan
[57] Department of Physics, Graduate School of Science, Kyoto University, Kyoto, Japan
[58] Institut de Ciències de l'Espai (IEEE-CSIC), Campus UAB, 08193 Barcelona, Spain
[59] Institució Catalana de Recerca i Estudis Avançats (ICREA), Barcelona, Spain
[60] Department of Physics and Department of Astronomy, University of Maryland, College Park, MD 20742, USA
[61] Dipartimento di Fisica, Università di Roma "Tor Vergata", I-00133 Roma, Italy
[62] Department of Physics, Massachusetts Institute of Technology, Cambridge, Massachusetts 02138, USA

of the lensing galaxies. IR spectroscopy allowed for the redshift of the quasar itself ($z = 2.507$) to be directly measured (Lidman et al. 1999).

However, even before the redshifts of PKS 1830−211 or its lensing galaxies were known, attempts were made to model the source as a lens (Kochanek & Narayan 1992; Nair et al. 1993). Since photons for the source and the image take different paths to reach Earth, it is expected that there will be a light travel time difference and consequently a time delay between the photons that arrive from the different lensed images. That is, variations in the light curve of the SW source will have the same shape as those from the NE source but arrive later with a constant time delay and have a smaller magnitude, with respect to variations in the NE source. Assuming the same emission region at different frequency bands the time delay should be the same since strong gravitational lensing (macrolensing) is an achromatic process. Because PKS 1830−211 is a blazar that has shown variability in MeV-GeV bands (COMPTEL, EGRET, AGILE, *Fermi*) this opened up the possibility that this time delay can be measured in γ rays.

Modeling combined with redshift and time delay measures can be used to measure Hubble's constant (Blandford & Narayan 1992). On the other hand PKS 1830−211 is a compound lensing system, with possible microlensing/millilensing substructures besides the two foreground lensing galaxies at $z = 0.886$ and $z = 0.19$. Microlensing in the X-ray band is suggested by Oshima et al. (2001). An energy-dependent flux ratio of the PKS 1830−211 lens images is found in sub-mm bands as clearly associated with the γ-ray flare of June 2012 and varying with time (Ciprini 2012; Martí-Vidal et al. 2013).

A time delay of $\Delta t = 26^{+4}_{-5}$ days was measured from the light curves of the two lensed images by Lovell et al. (1998) with ATCA. They used the values of the delay obtained, along with the model of Nair et al. (1993), to measure Hubble's constant to be $H_0 = 69^{+16}_{-9}$ km s^{-1} Mpc^{-1}, which is consistent with the most recent measurements (Ade et al. 2014). Using molecular absorption features, Wiklind & Combes (2001) found a time delay of 24^{+5}_{-4} days, consistent with the value found by Lovell et al. (1998). More detailed modeling of the lensing system, using the time delay of $\Delta t \approx 25$ days find similar values of H_0 (e.g., Lehár et al. 2000; Witt et al. 2000). A different time delay of $\Delta t = 44 \pm 9$ days was measured from the radio light curves of the two lensed images by van Ommen et al. (1995) using the VLA. Lovell et al. (1998) attribute the difference between their measured time delay and the one found by van Ommen et al. (1995) as being caused by "not correctly accounting for the contribution of the Einstein ring flux density when calculating the magnification ratio".

PKS 1830−211 is the brightest gravitational lens in the sky at centimeter wavelengths, hard X-ray and MeV energies. *Chandra*, XMM *Newton*, *Swift* BAT and INTEGRAL have measured very hard spectra ($\Gamma_{\rm X} \sim 1$) and high absorbing column densities accounting for a spectral break below ~ 4 keV(de Rosa et al. 2005; Foschini et al. 2006; Zhang et al. 2008).

PKS 1830−211 was detected by COMPTEL (Collmar 2006) in the 0.75−30 MeV band, by EGRET (above 100 MeV, 3EG J1832−2110; Mattox et al. 1997a; Combi & Romero 1998; Hartman et al. 1999; Torres et al. 2003) and more recently by AGILE (Striani et al. 2009; Donnarumma et al. 2011, and references therein).

It can be found in the first and second *Fermi* LAT source catalogs (1FGL J1833.6−2103, 2FGL J1833.6−2104, Abdo et al. 2010a; Nolan et al. 2012) with formal significances of about 41σ and 67σ, respectively. The radio source PKS 1830−211 and the intervening galaxies are within the LAT error ellipse, as a few nearby field galaxies; nevertheless, there is no source other than PKS 1830−211 with radio flux density $\gtrsim 10$ mJy, making it the source of γ rays.

Although the NE and SW images of PKS 1830−211 cannot be resolved by the LAT, the emission from the two images in principle can be distinguished by measuring a time delay from variable γ-ray light curves. This possibility was studied by Barnacka et al. (2011), who reported a 27.1 ± 0.6 day time delay found in the LAT light curve of this source. This value is in agreement with values found in the radio band (e.g. Lovell et al. 1998; van Ommen et al. 1995; Wiklind & Combes 2001).

PKS 1830−211 is an FSRQ characterized by a marked γ-ray Compton luminosity dominance (EGRET/COMPTEL observations, Collmar 2006). The broadband νF_ν spectral energy distribution (SED) has been modeled with a combination of synchrotron, synchrotron self-Compton (SSC), and external Compton (EC) scattering of dust torus photons assuming the broadband data were magnified by a factor of 10 by the lens (de Rosa et al. 2005). Foschini et al. (2006) and Celotti & Ghisellini (2008) modeled this source without correcting the SED data for extinction or magnification, which are not well known, and used the broad-line region (BLR) as the main seed photon source. Both models provide reasonable descriptions of this object. Hadronic models predict neutrino production coincident with γ-ray flares, and this motivates searches for neutrino events coincident with LAT flares (e.g. Cruz et al. 2013).

An outburst observed from the γ-ray point source positionally consistent with PKS 1830−211 was observed by *Fermi* LAT in 2010 October (Ciprini 2010). This is the largest flare observed since the beginning of the *Fermi* survey, and triggered rapid-response target of opportunity (ToO) observations by the *Swift* satellite[63]. AGILE also reported a high flux measurement obtained from 2010 October 15 through 17 (Donnarumma et al. 2011, and references therein).

In this paper, we explore the γ-ray properties of PKS 1830−211 as observed by the *Fermi* LAT, with particular attention paid to the main outburst of 2010 October and the second brightest flaring period (2010 December - 2011 January, Section 2). In Section 3 we discuss the γ-ray flux light curve and the search for time-lag signatures, an indicator of gravitational lensing. The *Swift* observations and results are presented in Section 4 and the multifrequency SEDs and spectral modeling are reported in Section 5. We conclude in Section 6.

2. *FERMI* LAT OBSERVATIONS

The *Fermi* LAT analysis was performed with the standard LAT `ScienceTools` software package (version v9r23p1) and was based on data collected in the period from 2008 August 4 to 2011 July 25 (from MJD 54682.65 to 55767.65, almost 3 years). We first produced a LAT spectrum for PKS 1830−211 over this entire time interval, using only the event class designated as P6_DIFFUSE (class==3), with corresponding P6_V3_DIFFUSE instrument response functions

[63] thanks to a Guest Investigator program *Swift* Cycle AO-6 for flaring LAT blazars (PI: L. Reyes)

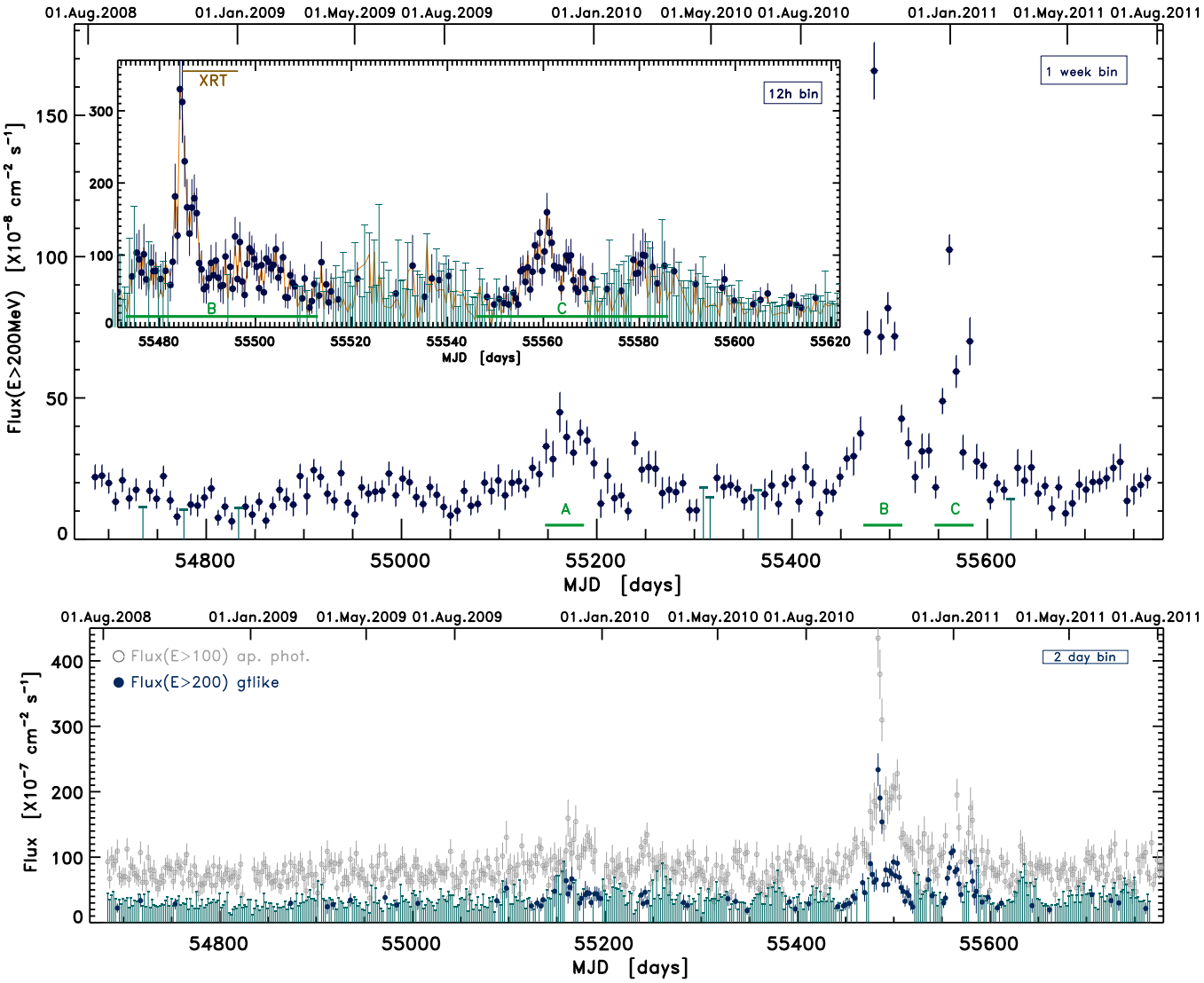

FIG. 1.— *Top panel*: 3-year (1085 days) LAT γ-ray flux ($E > 200$ MeV) light curve of PKS 1830−211 in weekly bins, extracted with `gtlike` fit in each bin from 2008 August 4 to 2011 July 25 (MJD 54682.65 to 55767.65). *Top inset panel*: `gtlike` light curve detailing the ~ 150 day period (MJD interval: 55471-55621, i.e. from 2010 October 2 to 2011, March 1) flux light curve extracted with 12-hour bins and containing the "B" and "C" intervals when the main outburst of 2010 October and the second largest, and double-peaked, flare of 2010 December and 2011 January occurred. In both panels vertical lines refer to 2-σ upper limits on the source flux. Upper limits have been computed for bins where $TS < 4$, $Npred < 3$, or $\Delta F_\gamma > F_\gamma/2$. *Lower panel*: 1° aperture photometry flux ($E > 100$ MeV) and `gtlike` flux ($E > 200$ MeV) light curve of PKS 1830−211 in 2-day bins for comparison.

(IRFs, Ackermann et al. 2012) [64], and selecting events in a circular Region of Interest (RoI) with 7° radius centered on the target position from the second *Fermi* source catalog 2FGL catalog. To reduce contamination from diffuse Galactic emission and nearby point sources, a low-energy cut of 200 MeV was used (compared to the usual cut of 100 MeV where the PSF is relatively large). A high-energy cut of 100 GeV was also implemented.

To avoid the contamination due to the γ-ray bright Earth limb in our analysis, all events with zenith angle $> 105°$ were excluded. Time intervals when the Earth entered the LAT Field of View (FoV) are excluded selecting only photons with spacecraft rocking angle $< 52°$. The unbinned maximum likelihood technique (`gtlike` tool) accounted for all the 21 neighboring sources and the diffuse emission in the physical model of the RoI together with the target source. The RoI model is fit to the data assuming for the source PKS 1830−211 a power-law spectrum between minimum and maximum energies (E_{min} and E_{max} respectively), $dN/dE \propto E^{-\Gamma_\gamma}$ with γ-ray photon index Γ_γ left free in the fit. A more complex log-parabola model is reported in the 2-year accumulated data of the 2FGL catalog (Nolan et al. 2012) for PKS 1830−211, but for the purposes of our study and the extraction of flux light curves in much shorter time bins, the power-law shape is found to reproduce adequately the source spectrum (the spectral parameter values obtained with the different models agree within the statistical errors and the difference in flux values is found to be on average 5%).

Source positions were fixed. The Galactic (`gll_iem_v02.fit`) and the isotropic

[64] These event class and IRFs were used to better compare our results with those of Barnacka et al. (2011), where a 2-day bin aperture photometry light curve of PKS 1830−211 (300 MeV - 30 GeV flux) was extracted from LAT data with P6_V3_DIFFUSE IRFs from 2008 August 4 through 2010 October 13.

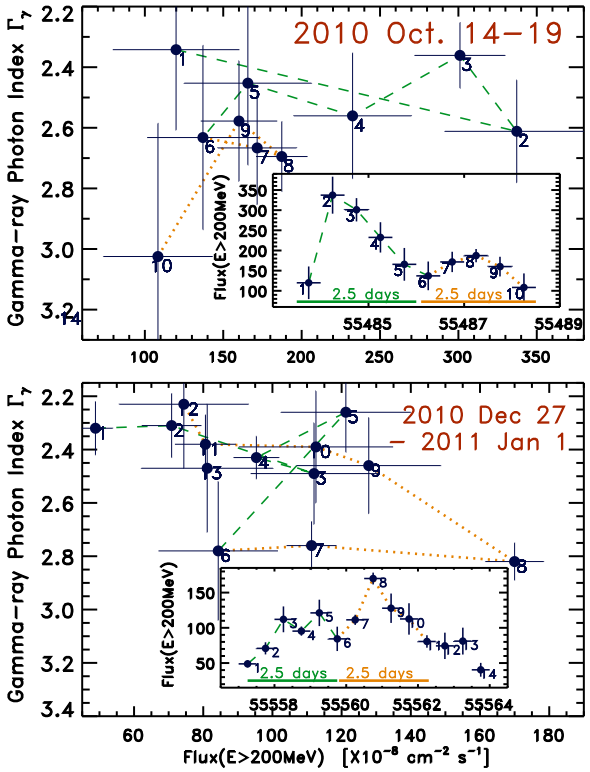

FIG. 2.— 5-day zooms on the evolution of the γ-ray photon index of PKS 1830−211 as a function of the γ-ray flux during the highest flux peaks of the two main flare events for the source (top and bottom panels). These peaks are contained in the "B" and "C" intervals of the 12-hour bin light curve reported in top inset panel of Figure 1. Here the photon index parameter is left free in the likelihood fit. Bars represent 1σ errors.

(`isotropic_iem_v02.fit`) background models[65] were used with their normalizations left as free parameters in each time bin, facilitating reliable convergence of the likelihood model fits and a reduced computational time. This procedure was the same as in previous works (e.g., Tanaka et al. 2013). The isotropic component included both the contribution from the extragalactic diffuse emission and from the residual charged-particle backgrounds. In addition, all γ-ray sources up to 10° around the target were included in the fit with power-law spectral models. The normalization and the photon index were left free for each point source within a 5° radius of PKS 1830−211. Sources between 5° and 7° had just their normalizations free (using for each source the fixed photon index reported in the 2FGL catalog), while sources within 7° and 10° had all parameters fixed. By exception, the pulsar PSR J1809−2332 was modeled with an exponentially cutoff power-law in which the photon index at low energy, the cutoff energy, and the normalization factor were left free. The power-law fit to PKS 1830−211 over the entire period in the $0.2 - 100$ GeV energy range gave an integrated flux of $(20.4 \pm 0.4)\times10^{-8}$ ph cm^{-2} s^{-1} and a steep γ-ray photon index of $\Gamma_\gamma = 2.55 \pm 0.02$.

Next, we produced a flux light curve for PKS 1830−211 using a bin-by-bin maximum likelihood fit (`gtlike` tool) in the 200 MeV - 100 GeV energy range with regular time intervals (12 hours, 2 days and 1 week). We did this assuming the simplest appropriate model, the power-law spectrum, by freezing the photon index for this source in the individual time bins equal to the value obtained for the spectral fit over the entire time range, $\Gamma_\gamma = 2.55$. This simplification reduced flux error bars produced by the fit minimization process. Figure 1 (top panel) shows the weekly (7-day bins) γ-ray light curve for about the first 3 years of the *Fermi* all sky survey. In the inset panel a 12-hour bin light curve was produced with the likelihood analysis for the 150-day long time interval going from 2010 October 2 (MJD 55471) to 2011 March 1 (MJD 55621) containing the main period of activity for the source with the outburst of 2010 October and the second largest flare of 2010 December and 2011 January. The lower panel of Figure 1 shows the 2-day bin likelihood flux light curve, mostly characterized by flux upper limits outside the periods of source activity. For these light curves upper limits have been computed for bins where $TS < 4$, the number of events predicted by the model, $N_{pred} < 3$, or the error on the flux, $\Delta F_\gamma > F_\gamma/2$. Here TS is the test statistic, defined as $TS = 2\Delta\log(\mathrm{Likelihood})$ between models with the additional source at a specified location and without an additional source, i.e., the "null hypothesis" (Mattox et al. 1996).

We further calculated flux (100 MeV to 200 GeV) light curves in regular time bins (12 hours and 2 days) using the aperture photometry technique (see, e.g., Hadasch et al. 2012) for the $\sim$ 3-year range (Figure 1, lower panel, light gray symbols). These flux estimations are extracted using the `gtbin` tool with an aperture radius of 1°, and are exposure corrected through the `gtexposure` tool assuming the power-law spectral shape and the same cuts to photon events reported above. The aperture photometry light curves include a rough background subtraction but, due to the large PSF of the LAT and the nature of the diffuse γ-ray emission, significant background contamination can be expected as can be seen by the higher "quiescent" level with respect to peak of the flares and the level of fluctuations.

The statistical treatment of the likelihood analysis performed in each time bin is the more rigorous approach to extract LAT light curves because of the complications related to the LAT instrument's energy-dependent PSF, geometry-dependent effective area, the nature of the γ-ray sky backgrounds, the all-sky survey operation mode, and the limited detection rate characterizing GeV γ-ray data. `gtlike` flux light curves provide greater sensitivity and lead to more accurate flux measurements as backgrounds can be modeled out and detailed spectral models can be applied. However, exposure corrected aperture photometry is a useful method for comparisons. It is model independent and more efficient, using short time bins through fewer analysis steps and reduced computational time.

We explore the γ-ray variability properties further in Section 3 (and Figures 1 - 4) with particular attention to possible lensing signatures.

3. GAMMA-RAY TIME VARIABILITY AND LENSING PROPERTIES

Our analysis is based on the maximum likelihood flux light curves (`gtlike` tool) while aperture photometry was used to produce supplemental light curves for comparison with the former. In Figure 1 we show the maximum likelihood flux ($E > 200$ MeV) light curve of PKS 1830−211 in regular weekly bins over the first 3 years of *Fermi* operation (2008 August 4 to 2011 July 25, MJD 54682.65 to 55767.65). Where $TS < 4$, $Npred < 3$, or $\Delta F_\gamma > F_\gamma/2$, 2-$\sigma$ upper limits on the source flux were computed. 1° aperture photometry flux ($E > 100$ MeV) and likelihood flux

[65] LAT background models:
`fermi.gsfc.nasa.gov/ssc/data/access/lat/BackgroundModels.html`

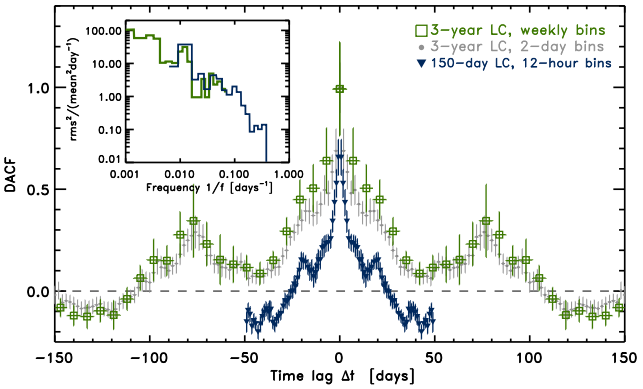

FIG. 3.— *Main panel*: Discrete autocorrelation function (DACF) of the 3-year, weekly bin (green square open points) 2-day bin (tiny light gray points) and 150-day, 12-hour bin (blue small triangles) LAT flux light curves shown in Figure 1. *Inset panel*: Power density spectra, PDS, normalized to fractional variance per frequency unit f calculated for the 3-year weekly and the 150-day, 12-hour bin LAT light curves.

($E > 200$ MeV) light curves, both with 2-day bins, are reported (bottom panel of Figure 1). A likelihood flux light curve in 12-hour bins is also extracted for the $\sim$ 150-day interval of the most active phase for the source ("B" and "C" intervals, upper inset panel). Aperture photometry 3-year light curves (1-day/2-day bins) are also extracted in different positions using non-PKS 1830−211 photons within the ROI, both along and outside the ecliptic path to better understand possible spurious effects caused by the Sun and Moon passages. We used the same event class and IRFs (P6_V6_DIFFUSE) used in Barnacka et al. (2011) with more checks using P6_V11_DIFFUSE IRFs, but different energy range selection (200 MeV - 100 GeV) and different variability analysis and time bin sizes.

The "A" interval contains the first γ-ray brightening seen by the LAT, near the end of 2009. The announcement of a detection by AGILE on 2009 October 12 and 13, MJD 55116-55117 (Donnarumma et al. 2011, and references therein) occurred already some weeks before the "A" interval.

To explore the behavior of PKS 1830−211 during the main outburst (interval "B") and the second brightest flaring period (interval "C") in greater detail, we performed power-law fits to the source in 12-hour bins, with both the flux and photon indices (Γ_γ) left as free parameters. This is in contrast to the likelihood light curves in Figure 1 where Γ_γ was fixed. Note that 12 hours corresponds to $\sim$ 8 *Fermi* orbits, so that exposures from bin to bin are roughly the same. The results can be found in Figure 2, where we searched possible spectral trends.

The top of Figure 2 shows the two largest peaks of structured outburst (within the "B" interval) of 2010 October. This is characterized by a rapid increase of a factor of ~ 2.6 in flux in 12 hours between 2010 October 14 and 15 (MJD 55483 and 55484) peak of $F(> 200\ \mathrm{MeV}) = (330 \pm 42) \times 10^{-8}$ ph cm^{-2} s^{-1} in $\sim$ 12 hours, yet taking $\sim$ 48 hours to fall, resulting in an asymmetric temporal shape. The total peak pulse lasts ~ 2.5 days, and seems to be followed by another weaker peak also lasting ~ 2.5 days. Both peaks do not show significant rotation in the Γ_γ-flux hysteresis diagram, because of the statistically constant photon index and relatively large uncertainties on flux and Γ_γ with respect to the variations.

The hysteresis diagram for flare "C", which occurred between about 2010 December 25 and 2011 January 6 (MJD 55555 - 55567) is seen in the bottom of Figure 2. This flare displays a temporal structure characterized by two peaks of about 2.5 days duration each. The second peak reaches a flux value of $(159 \pm 27) \times 10^{-8}$ ph cm^{-2} s^{-1}, roughly half of the peak flux of the "B" flare. The flare softens significantly (bins 6, 7, and 8 in the bottom of Figure 2) to $\Gamma_\gamma \sim 2.8$, before turning to its typical spectrum of $\Gamma_\gamma \sim 2.4$ during the decay.

Variability on timescales ranging from about two months down to a couple of days is seen in these LAT γ-ray light curves. Two power density spectra (PDS) normalized to fractional variance per unit frequency ($f = 1/t$) (rms^2 I^{-2} Day^{-1}), are shown in the inset panel of Figure 3. One is calculated from the 3-year and weekly light curve and one from the 12-hour bin light curve extracted for 150 days between 2010 October 2 (MJD 55471) and 2011 March 1 (MJD 55621) (top main and inset panels of Figure 1 respectively). Following Abdo et al. (2010b), we consider time bins with flux upper limits replaced by a value (10^{-12} ph cm^{-2} s^{-1}), i.e. below the LAT detection limits. This allows us to evenly sample the light curve and limit the bias caused by data gaps. The fraction of upper limits was 5% and 9% for the weekly and 12-hour bin light curves, respectively. Different choices (e.g. replacing upper limits with their half-limit values), affect the PDS slope estimates by a few percent, which is substantially less than other uncertainties. The white noise level was estimated from the rms of the flux errors and was subtracted for each PDS.

Both PDS are in good agreement with each other, meaning that the fractional variability and its time scale distribution during the more active "B" and "C" epochs are the same as during the longer and fainter periods between the flaring events. The merged PDS is fit with a simple $1/f^\alpha$ power law, with a slope $\alpha = 1.25 \pm 0.12$, while the low-frequency PDS is fit with $\alpha = 1.1 \pm 0.2$, and the high frequency one with $\alpha = 1.3 \pm 0.2$.

The main panel of Figure 3 reports the Discrete Autocorrelation Function (DACF) for the three likelihood flux light curves reported in Figure 1: the 3-year weekly and 2-day bin, the 150-day 12-hour bin light curves. The weekly and 2-day bin light curves follow the same function profile, consistent with the PDS power-law index, showing no signal power peak for timescales shorter than peak hinted at 76 ± 4 days. The origin of this value could be time series noise or related to the time between the "B" and "C" flare peaks. The control aperture photometry light curves for non-PKS 1830−211 photons extracted in different positions within the RoI do not provide signals at any timescale.

The DACF of the best-sampled 12-hour bin light curve shows a clearer peak of 19 ± 1 days that is not evident in the 2-day bin DACF. That value could represent a possible characteristic timescale of the time series, created by a regular gravitational lensing time delay as found in Barnacka et al. (2011). This might represent a possible point of rough agreement with their results. On the other hand this DACF peak can be produced by the timescale of the two main flare events (the peaks in the "B" and "C" intervals, Figures 1 and 2). A power spectrum analysis that is time-localized along the light curve epochs, like the wavelet method, can help to shed light on this. The 150-day duration, 12-hour bin, light curve was also analyzed using a Continuous Wavelet Transform (CWT) analysis (Figure 4). By decomposing the light curve into time-frequency (t, $f = 1/t$) generalized Fourier spaces, we are able to determine both the dominant modes of variability (as with the PDS), as well as how those modes vary in

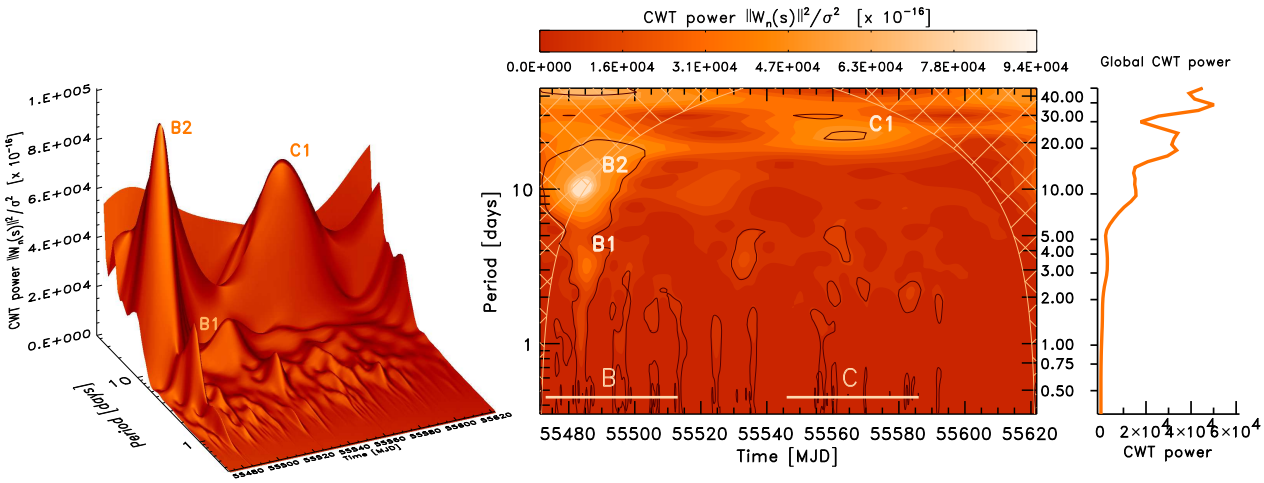

FIG. 4.— *Left panel*: plane contour plot of the continuous wavelet transform power density spectrum (2D PDS from CWT) for the 150-day and 12-hour bin light curve of Figure 1 (inset panel), obtained using a Morlet, complex valued, mother function. Filled color contour plot is the 2D energy density function of the CWT scalogram. Thick black line contours represents the 90% confidence levels of true signal features against white and red noise backgrounds, while cross-hatched regions represent the "cone of influence", where effects caused by finite time-series edges become important. *Right panel*: the average of the CWT scalogram over all times is reported, this consists in a smoothed time-averaged 1D CWT spectrum that is called global wavelet spectrum.

time, localizing them along the light curve epochs. This produces a diffuse and continuous two-dimensional (2D) time-frequency (or time-period) image plot, "the scalogram" (Fig. 4, left and central panels). In such a plot we report the normalized 2D modulus of the CWT energy density function ($\|W_n(s)\|^2/\sigma^2$, where the normalization $1/\sigma^2$ gives a measure of the power relative to white noise), computed using a Morlet mother waveform. This mother function provides the best tradeoff between time-localization and period (frequency) resolution. Thick black line contours are the 90% confidence levels of true signal features against white and red noise backgrounds, while cross-hatched regions represent the "cone of influence", where spurious edge effects caused by finite time-series boundaries become important.

Most of the CWT power, not influenced by edge effects, is concentrated within the period scales (y-axis) ranging from 8 to 30 days, even if there is appreciable power at longer periods (e.g., at 40-50 days). The main outburst ("B") is decomposed and resolved in time/frequency (x-y) spaces with the bulk of the power released between about MJD 55475 and 55495 (2010 October 6 - 26) peaking at MJD 55484 (2010 October 15), in agreement with the light curve shape. The corresponding characteristic scale is 10 days, which is related to the peak duration. The outburst is also characterized by a resolved timescale component of $\sim$ 3 days at MJD 55486 (October 17) in agreement with the 2.5-day peaks substructures mentioned (Fig. 2, top panel). This timescale still appears significant but drifted to longer values of about 3.5 days and 4.5 days respectively during the events at around MJD 55535 (2010 December 5) and MJD 55563 (2011 January 2, i.e. the flare epoch "C"). This second brightest flare event for PKS 1830−211 is identified by a significant (within 90% confidence local region) and well-defined peak of CWT signal power with characteristic timescale of about 21 days, between about MJD 55560 and 55565 (2010 December 30 and 2011 January 4) in agreement with the previous description and Figures 1 and 2 (bottom panel).

Summarizing, between the main outburst "B" and the second brightest flare "C", we observed a shift from a characteristic timescale of the main outburst of $\sim$ 10 days ("B2" peak in the CWT plot) to a timescale of $\sim$ 20 days for the second flare event ("C1" peak in the CWT plot). This suggests the "C" flare phase has twice the duration of the "B" flare phase, yet is approximately half as bright in emitted γ-ray power. The CWT analysis implies both these timescales are characteristic of the coherent and separate flare events "B" and "C". It does not provide evidence for a detection of a regular signal recurrent along the whole light curve as produced by gravitational lensing.

Based on a time delay of $\Delta t = 26^{+4}_{-5}$ days measured by Lovell et al. (1998) and 24^{+5}_{-4} days measured by Wiklind & Combes (2001), the main outburst "B", beginning between 2010 October 14 and 15 (MJD 55483-55484), should have a delayed event occurring within the time interval MJD 55503 - 55514 (2010 November 3 - 14). If the delay measurement of 44 ± 9 days (van Ommen et al. 1995) is correct, this would put the γ-ray flare from the lens image starting around 2010 November 27 (MJD 55527 ± 9). A delayed γ-ray flare event would appear in the CWT scalogram as a clear peak of power, separated on the horizontal (time) axis by the time delay from the "B" and the "C" flares. Delayed flares should also be visible in the best-sampled 12-hour bin flux light curve (as found in the LAT light curve of S3 0218+35, lens B0218+357 Cheung et al. 2014), contrary to our findings. The few peaks in the CWT power spectrum at about 27 days after the flaring epochs are not significant. In any case, the chance coincidence of two flares within 20–30 days has a non-negligible probability. A detection of a feature in the DACF such as the 19-day peak does not provide enough evidence of a detection of delayed events induced by lensing, as testified by the lack of a well-resolved peak in the epoch-averaged (global) CWT power spectrum (third, right panel of Figure 4).

Exposure-corrected aperture photometry provides supplementary information (Figure 1), even if the technique is limited by lower sensitivity, inaccuracies in the definition the model for diffuse γ-ray emission, small aperture area (and so also fewer photons from the source).

The unbinned likelihood potentially offers greater sensitivity, more accurate flux measurements, and reduced uncertainties and fluctuations. Both methods can be affected by spurious instrumental modulations and systematic errors. One possible effect is correlated to the dependence of the particle background rate on the *Fermi* spacecraft geomagnetic loca-

tion, which is modulated by the orbit precession[66]. Lunar γ-ray emission may influence every light curve extraction for PKS 1830−211 (Corbet et al. 2013). The ~ 27 day scale can be consistent both with the first harmonic of the *Fermi* spacecraft orbit precession period and the Moon's sidereal period. The comparison aperture photometry light curves extracted from non-PKS 1830−211 positions in our data do not show any significant signatures of such effects.

We note that changes in observing conditions and other instrumental effects could induce temporal correlations in measured quantities. Therefore, uncertainties in both the light curve and derived model parameters might be underestimated owing to the potential for additional low-level sources of systematic temporal correlations.

The absence of clear evidence for delayed flare episodes following the "B" and "C" events, and the lack of regular time scale signatures in our 3-year LAT data, imply either that lensing delayed flares at γ-ray energies do not exist in this source, or the flux ratio in the γ-ray band does not match that observed in the radio bands (~ 1.5). We might also be observing a time-dependent or energy-variable lensing flux ratio. A varying ratio (range 1.0 - 1.8) of the measured flux of the two radio images is already suggested in Wiklind & Combes (1998). Multi-year monitoring of the absorption caused by the $z = 0.886$ galaxy showed temporal changes in absorption lines, ascribed to motion of the blazar images with respect to the foreground galaxy and produced by sporadic ejection of bright plasmons (Muller & Guélin 2008). We discuss our result further in Section 6.1.

4. *SWIFT*: DATA ANALYSIS AND RESULTS

The *Swift* satellite (Gehrels et al. 2004) performed 10 ToO observations on PKS 1830−211 between 2010 October 15 (16:26 UT) and October 27 (09:07 UT), MJD 55484.685-55496.380, for a GI program triggered by the high γ-ray activity of the source. The *Swift* observations were performed with all three on-board instruments: the X-ray Telescope (XRT, 0.2–10.0 keV), the Ultraviolet/Optical Telescope (UVOT, 1700–6000 Å), and the Burst Alert Telescope (BAT, 15–150 keV).

4.1. Swift *BAT observations*

The hard X-ray flux of this source is below the sensitivity of the BAT instrument for the short exposures of the *Swift* ToO observations performed on 2010 October. The source was not detected between 2010 October 14 and 18 (net exposure of about 200 ks) by INTEGRAL (Donnarumma et al. 2011). By contrast, PKS 1830−211 is detected in the BAT 58-month catalog, generated from the all-sky survey from 2004 November to 2009 August. Therefore, we used the 8-channel spectrum available at the HEASARC[67]. The 14–195 keV spectrum is well described by a power law with photon index of 1.50±0.13 (χ^2_{red}/d.o.f. = 0.89/6). The resulting unabsorbed 14-195 keV flux is (9.0±0.8)×10^{-11} erg cm^{-2} s^{-1}. The difference in flux and photon index between the 58- and 70-month BAT catalog spectra is negligible.

4.2. Swift *XRT observations*

The XRT data were processed with standard procedures (`xrtpipeline` v0.12.4), including the filtering, and screening criteria from the `Heasoft` package (v.6.8). The source count rate was low during all the observations (count rate < 0.5 counts s^{-1}), so we only considered photon counting (PC) data and further selected XRT event grades 0–12. Source events were extracted from a circular region with a radius between 15 and 25 pixels (1 pixel $\sim 2.36''$), while background events were extracted from a circular region with radius 40 pixels away from background sources. Ancillary response files were generated with `xrtmkarf`, and accounted for different extraction regions, vignetting and PSF corrections. We used the the redistribution matrix function version v011 in the Calibration Database maintained by HEASARC. All spectra were rebinned with a minimum of 20 counts per energy bin to allow χ^2 fitting within XSPEC (v12.5.1).

Previous soft X-ray observations of PKS 1830−211 revealed a hard spectrum ($\Gamma_{\rm X} \sim 1$) and absorption in excess of the Galactic column due to the lensing galaxy at $z = 0.886$ (Mathur & Nair 1997; Oshima et al. 2001; de Rosa et al. 2005). In particular, de Rosa et al. (2005) derived a value of column density for this extra absorption of $1.94^{+0.28}_{-0.25} \times 10^{22}$ cm^{-2} from a broad band spectra with *Chandra* and INTEGRAL data. *XMM-Newton* observations of PKS 1830−211 were modeled by Foschini et al. (2006) with a broken power law model, with the photon index changing from ∼1.0 to ∼1.3 at about 3.5 keV. The joint fit of XMM/INTEGRAL data performed by Zhang et al. (2008) confirmed that the broken power law is the best model fit, with column density, photon indices and energy break parameters very similar to those found in the previously-cited works.

We fit the individual XRT spectra of 2010 October with an absorbed power law, with a neutral hydrogen column fixed to its Galactic value (2.05×10^{21} cm^{-2}; Kalberla et al. 2005) and an extra absorption fixed to the value found by De Rosa et al. (2005). The resulting unabsorbed 0.3–10 keV fluxes and the photon indices for each observation are reported in Figure 5. The unabsorbed flux derived from XRT observations lies between 1.3 and 1.7 × 10^{-11} erg cm^{-2} s^{-1}.

To investigate in more detail the X-ray spectral properties of the source we accumulated all the events collected during this campaign for extracting an average spectrum with higher statistics. As a first step we fit the average spectrum with the same model used for the single observations, obtaining an acceptable fit. Leaving the value of the column density of the extragalactic absorber free to vary, a comparable fit is recovered, with larger uncertainties on the parameters. We found instead an improvement in the fit substituting the simple power law with a broken power law model, significant at the 99.9% confidence level according to the F-test.

The 0.3–10 keV flux detected by XRT in 2010 October is only slightly higher than those observed in the past XMM-*Newton* and *Chandra* observations of the source (Table 1), indicating no significant activity in soft X-ray during the LAT flare.

A joint fit to the XRT+BAT spectrum with an absorbed broken power law and a cross-correlation factor between XRT and BAT of $1.30^{+0.36}_{-0.28}$ led to a further slight improvement (χ^2_{red}/d.o.f. = 1.09/133), with photon indices Γ_{X1} = 1.05±0.10 and Γ_{X2} = 1.53±0.11 below and above a break energy of $3.59^{+0.83}_{-0.51}$ keV.

4.3. Swift *UVOT Observations*

[66] Precession period of ~ 53.2 days as reported in Ackermann et al. (2012) and inferred from NORAD two-line element sets (`www.celestrak.com/NORAD/elements/`).

[67] `http://heasarc.gsfc.nasa.gov/docs/swift/results/bat`

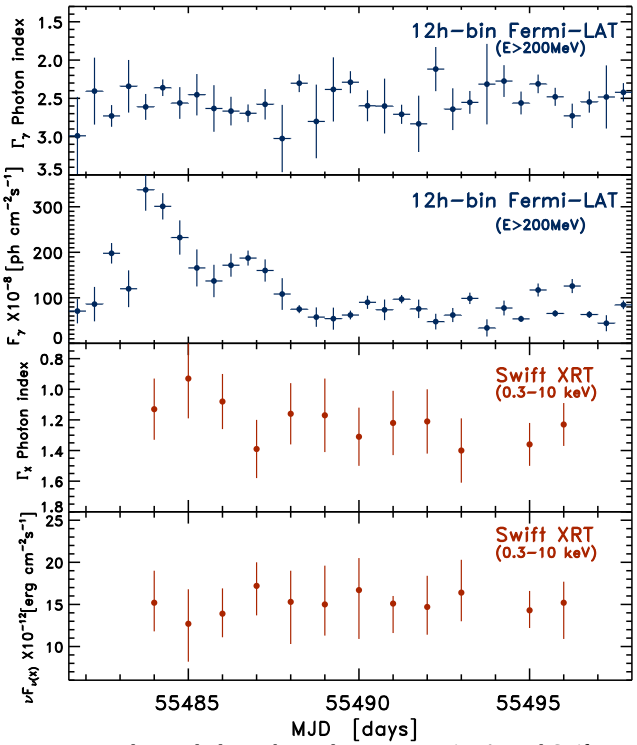

FIG. 5.— Multi-panel plot with simultaneous *Fermi* LAT and *Swift* XRT flux and photon index light curves.

TABLE 1
SUMMARY OF THE *Swift* XRT ANALYSIS OF THE PKS 1830−211 TOO OBSERVATIONS.

Power law Model				
Exp[a]	$N_{\rm H}$[b]	Γ_{X1}	Flux (0.3–10)[c]	$\chi^2_{\rm r}$/(d.o.f.)
20.3	1.94 (fix)	1.20 ± 0.06	1.64 ± 0.11	1.19 (129)
20.3	$2.09^{+0.54}_{-0.36}$	$1.23^{+0.11}_{-0.08}$	$1.65^{+0.27}_{-0.18}$	1.19 (128)
Broken Power law Model				
Exp[a]	$N_{\rm H}$[b]	Γ_{X1}/Γ_{X2}[d]	Flux (0.3–10)[c]	$\chi^2_{\rm r}$/(d.o.f.)
20.3	1.94 (fix)	1.05 ± 0.10	$1.53^{+0.14}_{-0.11}$	1.13
		$1.56^{+0.39}_{-0.20}$		(127)

(a) Net exposure in kiloseconds adding the single XRT observations performed between 2010 October 15 and 24.

(b) Column density of the extragalactic absorber at redshift z=0.886 in units of 10^{22} cm^{-2}. A Galactic absorption of 2.05×10^{21} cm^{-2} (Kalberla et al. 2005) is added.

(c) Unabsorbed flux in the $0.3 - 10$ keV energy band.

(d) $E_{\rm break} = 3.65^{+1.35}_{-0.60}$ keV.

During the *Swift* pointings, the UVOT instrument observed PKS 1830−211 in the v, b, u, and $uvw1$, $uvm2$ and $uvw2$ photometric bands. The analysis was performed using the `uvotsource` tool to extract counts from a standard 5″ radius aperture centered on the source, correct for coincidence losses, apply background subtraction and co-add all of the individual images for each filter. Nevertheless, due to the high extinction in the direction of PKS 1830−211, the source was not detected above 3-σ in any of the UVOT bands, so we computed a 3-σ flux upper limit (lower limit in magnitude) for each filter: $v > 18.0$, $b > 19.5$, $u > 19.3$, $uvw1 > 16.9$, $uvm2 > 20.0$, and $uvw2 > 21.0$.

5. BROADBAND SPECTRAL ENERGY DISTRIBUTION

The νF_ν SED of PKS 1830−211 around the 2010 October outburst (epoch "B") is shown in Figure 6. The data have been de-magnified by a factor of 10, following Nair et al. (1993) and Mathur & Nair (1997). Rarely can pure synchrotron/SSC models reproduce the observed SEDs of FSRQs. We attempted to fit PKS 1830−211 with such a model, but similar to de Rosa et al. (2005), we were not able to adequately reproduce its SED, since the SSC component is too broad to reproduce the X-ray and γ-ray data.

The high activity observed in γ rays has no significant counterpart in soft X rays, but those data can be described by a single EC component, suggesting that the X-ray photons originated in the low-energy tail of the same electron distribution. To fit the simultaneous 2010 October SED with an EC model, we assume that the emitting region is at a considerable distance from the black hole, outside the BLR, and that the primary seed photon source is from a dust torus emitting blackbody radiation in the infrared. There is some debate about the location of the γ-ray emitting region, although a large distance from the black hole seems justified for FSRQs by detailed campaigns by the *Fermi* LAT and radio observatories (e.g., Marscher et al. 2010). The dust torus was assumed to be a one-dimensional annulus with radius r_{dust} centered on the black hole and aligned perpendicular to the jet, and emitting blackbody radiation with temperature T_{dust} and luminosity L_{dust}. The dust parameters were chosen to be consistent with the sublimation radius (Nenkova et al. 2008). For the disk luminosity in our models, the BLR radius would be at 2×10^{17} cm, using the scaling relation of Ghisellini & Tavecchio (2008). We place the emitting region at a distance 10 times that of the BLR, making Compton scattering of BLR photons negligible (Dermer et al. 2009).

Our best fit is shown as the blue curve in Figure 6, and the parameters of the fit are described in Table 2. The entries in this table are free parameters except the jet powers and the blob radius. The model and parameters are described in detail by Dermer et al. (2009). The emitting region size scale chosen is consistent with a variability time scale of 12 hours, observed for the main outburst epoch ("B").

We found that an electron distribution with two spectral breaks (three power laws) was necessary to reproduce the SED. A very hard p_1 was necessary to fit the hard XRT spectrum. The other electron indices, p_2 and p_3, were chosen to be the same as the fit by de Rosa et al. (2005). Due to the simultaneous non-detection at UV/optical wavelengths, our model is not strongly constrained. Notice that the Compton-scattered peak is $\sim 10^3$ times larger than the synchrotron peak, and that this is really a lower limit on the Compton-dominance, due to the lack of an optical detection. For the outburst "B" SED fit, the total jet power, $P_{j,B} + P_{j,e} \approx 3.3 \times 10^{45}$ erg s^{-1} is below the Eddington luminosity for a 10^9 $M_\odot$ black hole ($L_{Edd} \approx 1.3 \times 10^{47}$ erg s^{-1}), as one would expect, and the magnetic field and nonthermal electrons are within approximately a factor of 4 from equipartition. Again, as with the fit by de Rosa et al. (2005), this fit is also able to explain the X-ray and γ-ray emission with a single EC component. The fit is also similar to the one by Foschini et al. (2006).

We also built a "quiescent state" SED of PKS 1830−211 from non-simultaneous data: the 58-month BAT spectrum, the *Planck* Early Release Compact Source Catalogue, ERCSC, spectrum, the LAT first-26 month spectrum. This LAT spectrum excludes the prominent flaring activity in 2010 October and 2010 December/2011 January, and so should be a

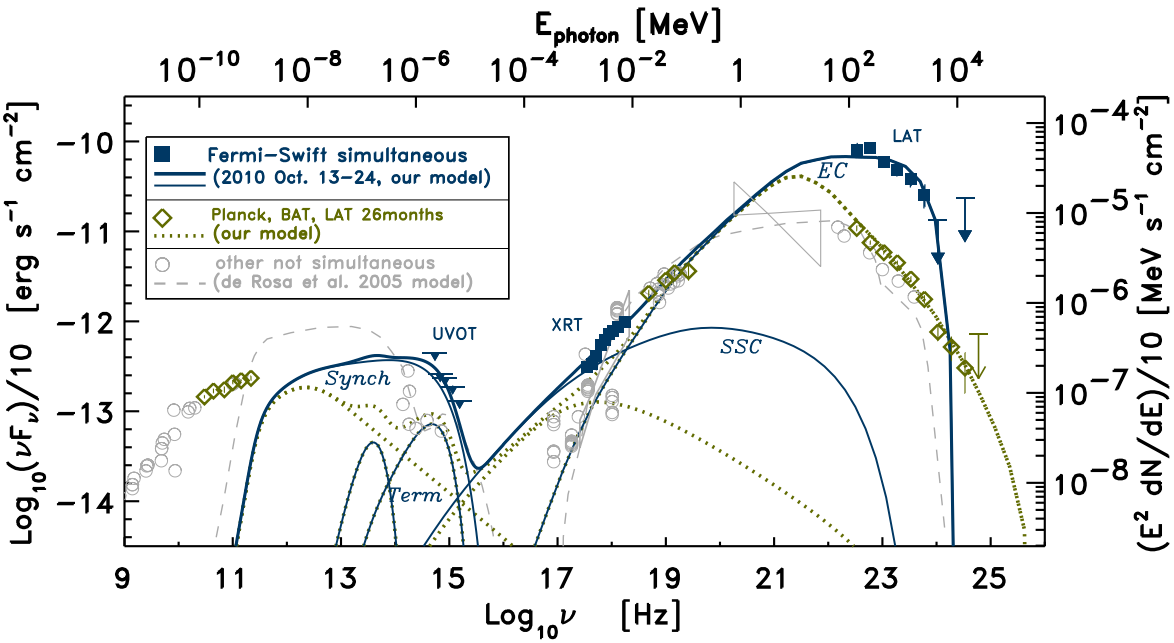

FIG. 6.— The SED of PKS 1830−211 built with simultaneous *Fermi* LAT and *Swift* XRT and UVOT (upper limits only) data, averaged over the 2010 October 13-24 campaign and corresponding to the γ-ray outburst (all plotted as blue/dark square symbols). Also plotted are a non-simultaneous 26-month LAT spectrum, the BAT 58-month spectrum, and the *Planck* ERCSC spectrum (all plotted as green/dark open diamond symbols). Archival data from radio/mm, Gemini-N, *HST*, *Chandra* (2001 January), INTEGRAL IBIS (2003), COMPTEL (bowtie), and EGRET are taken from literature (de Rosa et al. 2005; Foschini et al. 2006; Zhang et al. 2008) and are plotted as light grey open circles with a light gray dashed-line model. All data are corrected for lensing for a factor of 10 magnification (although note that the magnification may not be the same for all frequencies; see section 6.1). Also plotted are fits with a synchrotron/SSC/EC model to the outburst state (blue/dark solid curves fitting the LAT, XRT, UVOT simultaneous campaign data) and to the low activity state (green/dark dotted curves) represented by LAT, BAT, ERCSC not simultaneous data.

fairly good representation of the source during low-variability and low-activity states (green/dark data points with diamond symbol and dotted green/dark lines fit in Figure 6).

We also included the other relevant archival data (gray open circle data points in Figure 6, with instruments indicated in the caption). The dust and disk emission are the same for both models. We found that we could reproduce the quiescent state SED by varying only two parameters from the outburst state SED, namely the highest electron index ($p_3 = 4$) and the cutoff of the electron distribution ($\gamma_{max} = 10^5$). This attempt provides a decent fit to the archival data, except for the COMPTEL bowtie. However, since these are non-simultaneous, this should not be considered a major deficiency in the modeling. The archival optical emission here comes mainly from the accretion disk, so that this fit is also poorly constrained. Finally, the model fit from de Rosa et al. (2005) is shown for comparison. The model is quite similar to ours, although it provides a bit better fit to the archival optical and COMPTEL data.

6. DISCUSSION AND CONCLUSIONS

We have presented detailed *Fermi* LAT γ-ray and *Swift* observations of the gravitationally-lensed and MeV-peaked FSRQ PKS 1830−211. The LAT analysis was based on data collected in the period from 2008 August 4 to 2011 July 25 (from MJD 54682.65 to 55767.65, about 3 years). Increased γ-ray activity of this source was detected in 2009 November followed by a large outburst in 2010 mid-October, namely epoch "B", and a second flare at the period between 2010 December and 2011 January, namely epoch "C". PKS 1830−211 stands out for a number of reasons, besides the fact that it is characterized by strong-type gravitational lensing, which we discuss further in Section 6.1.

PKS 1830−211 is the third most distant object detected in large flaring activity so far by *Fermi* LAT behind TXS 0536+145 and B3 1343+451. The apparent isotropic γ-ray luminosity ($E > 100$ MeV) of PKS 1830−211 over the first 31 months of *Fermi* operation is $\sim 1.1\times10^{49}$ erg s^{-1}, comparable to the brightest high redshift ($z \gtrsim 2$) blazars in the Second LAT AGN Catalog (Ackermann et al. 2011, 2LAC).

The γ-ray flux observed by the LAT from this source was at its peak on 2010 October 14-15, reaching a flux of $F(E > 200\ \mathrm{MeV}) \approx 300 \times 10^{-8}$ ph cm^{-2} s^{-1}, as seen in the 12-hour binned light curve. This is a factor of 17 greater than the average 3-year flux. The corresponding apparent isotropic γ-ray luminosity of 2.9×10^{50} erg s^{-1} is greater than that observed from PKS 1622−297 during the 1995 flare (Mattox et al. 1997b), and from 3C 454.3 in 2009 December (Ackermann et al. 2010), and roughly comparable to the 2010 November outburst from this source (Abdo et al. 2011). For this bright flare, if one uses the variability timescale in the proper frame of the source $\Delta t \approx 12\,\mathrm{hours}/(1+\mathrm{z}) \approx 1.3\times10^4$ s, and a de-magnified luminosity of $L_\gamma \approx 3 \times 10^{49}$ erg s^{-1}, one calculates $L_\gamma/\Delta t \approx 2.5\times10^{45}$ erg s^{-2}. This value is a bit below the record-holder for AGN, from the 2010 November burst from 3C 454.3 (Abdo et al. 2011), but it still exceeds the Elliot & Shapiro (1974) limit of $L_{Edd}/(R_S/c) \approx 1.3 \times 10^{43}$ erg s^{-2} (where R_S is the Schwarzschild radius), and the limit that includes Klein-Nishina effects, 1.6×10^{44} erg s^{-2} (Liang & Liu 2003).

No correlated variability for this γ-ray flare was detected in X rays by *Swift* XRT, which is somewhat typical for FSRQs (e.g., Marscher et al. 2010; Hayashida et al. 2012), although not universal (e.g., Raiteri et al. 2011). Orphan γ-ray flaring activity in PKS 1830−211 was already found in AGILE data (Donnarumma et al. 2011). This fact, in addition to the lack

TABLE 2
MODEL FIT PARAMETERS

Parameter	Symbol	2010 Oct 13–24 fit	Quiescent fit
Bulk Lorentz Factor	Γ	20	20
Doppler Factor	δ_D	20	20
Magnetic Field	B	1 G	1 G
Variability Timescale	t_v	12 hours	12 hours
Comoving Blob radius	R'_b	7.4×10^{15} cm	7.4×10^{15} cm
Jet Height	r	10^{18} cm	10^{18} cm
Low-Energy Electron Spectral Index	p_1	1.0	1.0
Medium-Energy Electron Spectral Index	p_2	1.8	1.8
High-Energy Electron Spectral Index	p_3	2.8	4.0
Minimum Electron Lorentz Factor	γ'_{min}	3	3
First Break Electron Lorentz Factor	γ'_{brk1}	30	30
Second Break Electron Lorentz Factor	γ'_{brk2}	300	300
Maximum Electron Lorentz Factor	γ'_{max}	6×10^3	1×10^5
Black Hole Mass	M_{BH}	$10^9\ M_\odot$	$10^9\ M_\odot$
Accretion Disk Luminosity	L_{disk}	3.9×10^{P45} erg s^{-1}	3.9×10^{45} erg s^{-1}
Inner disk radius	R_{in}	$6R_g$	$6R_g$
Blob distance from black hole	r_{blob}	10^{18}	10^{18}
Dust torus temperature	T_{dust}	1.7×10^3 K	1.7×10^3 K
Dust torus radius	r_{dust}	2×10^{18} cm	2×10^{18} cm
Dust torus luminosity	L_{dust}	3.1×10^{45} erg s^{-1}	3.1×10^{45} erg s^{-1}
Jet Power in Magnetic Field	$L_{j,B}$	1.6×10^{44} erg s^{-1}	1.6×10^{44} erg s^{-1}
Jet Power in Electrons	$L_{j,e}$	3.8×10^{45} erg s^{-1}	3.1×10^{45} erg s^{-1}
Total Jet Power	$L_{j,tot}$	4.0×10^{45} erg s^{-1}	3.3×10^{45} erg s^{-1}

of detection in optical/UV by *Swift* UVOT and hard X-ray by INTEGRAL IBIS during the 2010 October γ-ray flare discovered by *Fermi* LAT, indicates the mechanism producing the γ-ray flare only marginally influences the X-ray part of the spectrum. There may be correlated variability between γ-ray and optical emission, also typical for FSRQs (e.g., Marscher et al. 2010; Raiteri et al. 2011), but without any optical detections, it is impossible to tell. The lack of X-ray and γ-ray correlation can support the lack of evident signals of strong lensing at high energies.

The hard and soft X rays are thought to be a combination of the contributions from SSC and EC, and the soft X-ray roll-off is explained in terms of a natural interplay between SSC and EC components (Foschini et al. 2006). The extremely hard X-ray photon indices have been found for a number of other blazars (Sikora et al. 2009), and seem to indicate very hard electron distributions at low energies.

The main ("B") outburst of 2010 October was found asymmetric with a fast rise of a factor about 2.6 in flux in 12 hours, a phenomenology observed in a few γ-ray blazar flares in the past (Abdo et al. 2010b). The asymmetry might imply particle acceleration and cooling times that are greater than the light crossing time, i.e., $t_{\rm inj}, t_{\rm cool} > R/c$ (in the jet comoving frame). The fast rise and slower decay shape can also be evidence for a contribution by Comptonization of photons produced outside the jet (Sikora et al. 2001; Sokolov & Marscher 2005).

A 2.5-day flux peak timescale appears to characterize the "B" and "C" flares. The main outburst "B" was characterized by a 10-day timescale, but there was a shift to a timescale of about 20 days during the "C" flare. That is, the timescale of the emission doubled. This is based on the 2D CWT scalogram for the 12-hour bin light curve, and is supported by the CWT global spectrum and the DACF (with a peak at 19 ± 1 days). This scale appears to be unconnected to a regular lens-delay signature running along the whole light curve: it is at the boundary of the range of the radio delay values ($\sim 20 - 30$ Lovell et al. 1998; Wiklind & Combes 2001) and would not be well compatible with the $\sim$ 27-day value found in Barnacka et al. (2011). In general multi-scale variability ranging from months down to a couple of days is found in the LAT light curves. In particular the 76-day interval separating the peaks of the two main flare episodes "B" and "C", namely the peak of 2010 October 15 (MJD 55484) and the peak of 2010 December 30 (MJD 55560) emerged as a possible signature from the DACF analysis. In terms of gravitational lensing this lag cannot be connected to radio-band lag values, and only one episode is not sufficient to make further speculations in this direction. The fractional γ-ray variability and its timescale distribution during the more active phases are found to be similar to the the ones shown in the longer, fainter and less variable intervals between the flare events, and the PDS can be described by a $1/f^{1.25\pm0.12}$ power law. This implies the occurrence of a specific variation is inversely proportional to its strength, with more weight preferred for short timescales.

The steep γ-ray spectrum of MeV-peaked sources like PKS 1830$-$211 can contribute to the cosmic X-ray background and the extragalactic γ-ray background, depending by luminosity functions as well as SED models. The 3-year LAT data analysis presented in this work suggests its γ-ray flaring activity and temporal behavior are due to intrinsic variability within the source, rather than to strong gravitational lensing effects. Data acquired in the next years of *Fermi* all-sky survey monitor will shed more light on the meaning of the hinted timescales.

6.1. *Why has no time delay been observed in gamma rays?*

The intense γ-ray flaring from PKS 1830$-$211, the brightest LAT gravitationally lensed blazar together with S3 0218+35 (i.e. the lens system B0218+357 Cheung et al. 2014), has opened up the possibility of measuring γ-ray time delays from the different lensed images of the blazar. The first clear γ-ray measurement of a delay for the images of the lens B0218+357 is reported in Cheung et al. (2014), where a lag of $\simeq 11.5$ days, that is ~ 1 day greater than previously determined radio-band values, was determined. Inspecting the intervals around the brightest flares of this source, magnifica-

tion flux ratios in γ-ray energy bands were measured oscillating about unity, with magnitudes smaller than those from radio observations. In the case of PKS 1830−211 however, as we show in Section 3, the expected delay of ≈ 25 days with a flux ratio ≈ 1.5 (e.g., Lovell et al. 1998) was not found by us with enough evidence, despite first claims to the contrary (Barnacka et al. 2011). We can set a lower limit of ~ 6 for the γ-ray flux ratio between the two lens images, significantly larger than the flux ratio in radio bands. The two radio images correspond to very slightly different viewing angles of the background blazar ($\Delta\theta \sim 1$ arcsec); therefore any source emission anisotropy, such as relativistic beaming, can change the observed flux ratio. This first limit found by us in γ-rays implies a very small beaming angle for the γ-ray emission.

PKS 1830−211 is a case of both strong lensing (characterized by a double image) and a compound lensing induced by two foreground galaxies. For an ideal lens the flux image ratios in different energy bands should be the same as the deflection is achromatic (Schneider et al. 1992). Multiple imaged quasars and blazars are expected to show intrinsic variability in all the resolved lensed images with the same time delay. Variable differences between the light curves could be ascribed to microlensing acting on the system. Inhomogeneities and radiation absorption can significantly change the observed flux and lensing magnification. In particular some material can interfere with the γ-rays in the lens galaxy and suppresses those from the SW image of PKS 1830−211. In Winn et al. (2002) the SW image of PKS 1830−211 is observed to pass through one of the spiral arms of the $z = 0.19$ foreground galaxy.

Different flux ratios have been measured from other lensed quasars (e.g., Blackburne et al. 2006; Pooley et al. 2006; Chen et al. 2011). Those authors attributed this to microlensing substructure in the lensing system and a different spatial origin of the emission at different wavelengths (X-ray and optical emission in those cases). This has been shown to be possible through lens modeling (Dobler & Keeton 2006) and can explain the observed different flux ratio with respect to the radio one. The amplitude of the magnification caused by microlensing is greater for small emission regions. Production sites for GeV γ-rays are generally much smaller than those at radio bands (< 0.003 pc from our SED modeling). Microlensing in the lens foreground galaxy could therefore produce further flux modulations and variations of the light curve produced by stellar motions in the galaxy. Optical microlensing is observed in some galaxies, and γ-ray emitting regions are comparable to the optical continuum size of an AGN. Based on EGRET data of PKS 1830−211 γ-ray flux variations are already suggested to be produced by gravitational microlensing (Combi & Romero 1998). Microlensing could allow to constrain the postulated power-law relationship $R \propto E^a$ between size and energy of γ-ray emission regions, and could explain some of the unidentified LAT γ-ray sources at high galactic latitude through lensing magnification of background undetected blazars (Torres et al. 2003).

The typical time scale for a caustic-crossing microlensing event in a lensed quasar however is longer than ~ 25 days (weeks, months Fluke & Webster 1999; Wambsganss 2001). On the other hand modeling of microlensing events has also shown that microlensing durations can be different for different wavelengths when the emission originates from different size scales (Jovanović et al. 2008). In addition PKS 1830−211 has rather fast source crossing times and a small ratio of source size to Einstein radius (Mosquera & Kochanek 2011), therefore significant microlensing variations are expected for this lensed γ-ray blazar.

The evidence for gravitational microlensing and millilensing effects in strong lensed quasars is increasing in recent works (e.g. Blackburne et al. 2011; Chartas et al. 2012; Chen et al. 2012). Microlensing structures or light path time delays sampling intrinsic quasar spectral variability are thought to explain optical spectral differences between quasar image components (e.g., Wisotzki et al. 1993; Sluse et al. 2007, 2013). In X-rays spectral variations can be described by changes of absorption column density, and by different spectral components and broken power laws, with different absorptions. It may be possible that the X-ray beam passes through a high-absorption column, but the radio band image is covered by a partial absorber with a low covering factor. In the peculiar case of PKS 1830−211, energy dependence observed in X-ray flux ratio between the two images is also ascribed to microlensing events Oshima et al. (2001) inducing time variability and X-ray chromatic perturbations. For example, X-ray microlensing variability was identified and disentangled in the *Einstein Cross* QSO 2237+0305 (Zimmer et al. 2011).

The observed flux of resolved lens images (i) at time t is a result of different factors: $F^{(i)}(t) = \mu^{(i)}_{macro} \cdot \mu^{(i)}_{micro} \cdot Q(t)\mu^{(i)}_{macro}$, where μ are the macro/micro-lensing magnification factors and $Q(t)$ the time-dependent flux of the quasar. The Einstein-ring radius on the PKS 1830−211 source plane is $R_E = \theta_E D_{os} \simeq 2 \times 10^{16}\sqrt{M_{lens}/M_\odot}$ (Paczynski 1986; Oshima et al. 2001).

We can use the lower limit of ~ 6 in the γ-ray flux ratio to put an upper limit on the size of the γ-ray emitting region (Grieger et al. 1991; Yonehara et al. 1998). We find that this must be $R'_b \lesssim 5.6 \times 10^{14} m^{1/2}$ cm, where m is the mass of a microlens in solar masses. This is consistent with the γ-ray variability timescale, although it is larger than the size used in SED modeling (section 5). The size of the γ-ray emission region evaluated from the SED modeling (7.4×10^{15} cm) is smaller than R_E and is therefore subject to possible microlensing, inducing magnification variations with respect to radio wavelengths where the emission region is more extended. In particular a larger magnification ratio is expected for a caustic-crossing microlens event (Blandford & Narayan 1992) acting on one of the two images, as suggested by the $\gtrsim 6$ γ-ray flux ratio. It should be noted that microlensing due to individual stars in the main lens galaxy is expected to be negligible in many cases, as the projected Einstein radius of each star is smaller than the PKS 1830−211 optical source extension. However, further lensing effects can be due to nearby galaxies. There are six other secondary galaxy candidates for weak lensing, identified in the field within 20" from the main lens by Lehár et al. (2000). These galaxies can provide lensing effects exerted at the position of the NE and the SW images of PKS 1830−211, in the case that one or more of them is relatively massive and placed at $z \lesssim 0.1$. In this case they would have to be included in PKS 1830−211 lens modeling.

Besides micro/milli-lensing effects and the need for a refined strong lensing modeling, there are other open possibilities that could explain the lack of an evident γ-ray lensing time delay for the two major flares of PKS 1830−211 seen by the LAT. *Chandra* and XMM-*Newton* observations of PKS 1830−211 show large variations in the absorption column density, which are interpreted as intrinsic absorption (Dai et al. 2008). As the PKS 1830−211 X-ray emission is

dominated by relativistically beamed components from the jet, it is very likely that the obscuration may be due to jet-linked absorbing material, physical processes, or variations from the geometric configuration of the jet. If the γ-ray emission region is displaced from the radio-band emission region the γ-ray flux ratio can have the observed difference from the radio flux ratio. Spatially distinct emission regions may give some constraint on differing jet structure probed by the two different energy regimes. This hypothesis may complicate results for this blazar in comparing the radio/γ-ray properties, in evaluating Compton dominance, and in correctly modeling its SED. It could be possible that the radio and γ-ray emission in blazars comes from different regions of the jet with different size scales. This is due to the well-known fact that variability at these different wavelengths is on considerably different timescales, and that compact synchrotron emission from jets is strongly self-absorbed at radio frequencies. The γ-ray emission site for the quiescent period from August 2008 to September 2010 and the γ-ray emitting region responsible for the two main flaring episodes "B" and "C" also could be different (Barnacka et al. 2014) with different lensing magnification ratios. In general the magnification ratio might differ for radio-band and γ-ray emission, especially when there are high-energy flaring episodes.

Multi-epoch and multi-frequency continuum observations of the two resolved lensed images of PKS 1830−211 by ALMA in the 350-1050 GHz band showed a remarkable frequency-dependent behavior of the flux ratio of the two images during the flare observed by the LAT in June 2012 (Martí-Vidal et al. 2013). This implies the presence of energy-dependent submillimeter structures in PKS 1830−211 during the γ-ray flare. While micro/milli-lensing events can already introduce a variability in the flux ratio, frequency-dependent changes directly imply an energy-dependent structure in the blazar nucleus like a "core-shift" effect (i.e. the frequency-dependent astrometric shift of the VLBI core position). This discovery can have direct consequences for our observations considering the supposed mm/sub-mm and GeV γ-ray connection in blazars (Giommi et al. 2012; Marscher et al. 2012). The concurrence and co-spatiality of the submm and γ-ray June 2012 flares is a direct prediction of the shock-injet model, while the remarkable energy dependence of the flux ratio of the two mm/submm core images is related to opacity effects close to the base of the jet (Martí-Vidal et al. 2013).

In radio bands dispersive refractive properties of the emitting plasma itself can cause gravitational deflection angle to be dependent by the photon energy (Bisnovatyi-Kogan & Tsupko 2010), but this effect can be considered not significant at GeV energies. Another aspect is the presence of a strong (cluster-scale) gravitational potential, even with strong lensing only. Source emission anisotropy may create spectroscopic differences along the slightly different lines of sight, yielding to differences in relativistic beaming of the images and a certain probability that one of the lensed image and delayed flare event may be not observable (Perna & Keeton 2009). However, the Einstein angle is small for an isolated galaxy scale potential and consequently also source anisotropy is not significant in the case of PKS 1830−211.

The non-detection of delayed flares for the "B" and "C" γ-ray flares and the lack of correlated activity in soft X-rays observed by *Swift* do not interfere with the association and identification of this LAT source with the lensed background blazar PKS 1830−211. This is because of the tighter spatial localization constraints towards PKS 1830−211 coming from the 1FGL, 2FGL (and the next 3FGL) Catalogs for the source. Additionally, the lensing galaxies located at $z = 0.88582$ and $z = 0.19$ are unlikely to be bright γ-ray sources, being a passive faint red galaxy and a passive face-on spiral galaxy (Courbin et al. 2002; Winn et al. 2002) respectively. The identification of PKS 1830−211 as a γ-ray source is declared since the EGRET era (Mattox et al. 1997a; Combi & Romero 1998).

Though initially considered a simple two-image gravitational lens, the lensed γ-ray quasar PKS 1830−211 appears to have several peculiar and intriguing features. The line of sight to PKS 1830−211 appears to be very busy: one possible Galactic main-sequence star, and two or (more likely) three lensing galaxies (Courbin et al. 2002). PKS 1830−211 represents also the first known case of a quasar lensed by an almost face-on spiral galaxy (Courbin et al. 2002; Winn et al. 2002), where a different flux suppression for the two different lens image paths represents another hypothesis.

No lens model has been able to explain yet all the observed characteristics and physical phenomena associated with the lens galaxies and the background blazar. As example the same radio time delay value ~ 26 days could be replaced by a more secure range of possible time delays ranging from 12 to 30 days, based on the full set of light curves used by Lovell et al. (1998). There is also evidence for substructure in this lens and the true mass distribution os the system is probably more complicated than the distributions in published lens models for PKS 1830−211 (Jin et al. 2003).

Deep optical imaging of PKS 1830−211 does not produce a clear picture of the lens and surrounding field because the line of sight lies near to the Galactic plane and the bulge of the Milky Way. Modeling of PKS 1830−211 has not been able to derive the Hubble constant with the precision obtained using other cosmological lenses. Besides uncertainty in the measured radio-time delay PKS 1830−211 has also remarkable uncertainties in the localization of the lensing galaxy and lens barycenter.

The continuous all-sky survey monitoring performed in the next years by *Fermi* LAT during the extended mission era, and the future Pass 8 data release, based on a complete revision of the entire event-level analysis, will allow the production of improved light curves for more detailed analysis. PKS 1830−211 may be the best high-energy gravitational lens for simultaneous mm/sub-mm and γ-ray variability and lensing studies with ALMA and the *Fermi* LAT.

7. ACKNOWLEDGMENTS

We thank the anonymous referees for useful comments that improved the paper. SC thanks Dr. R. Porcas of MPIfR, Bonn, Germany for a useful discussion during the course of this work. The *Fermi* LAT Collaboration acknowledges generous ongoing support from a number of agencies and institutes that have supported both the development and the operation of the LAT as well as scientific data analysis. These include the National Aeronautics and Space Administration and the Department of Energy in the United States, the Commissariat à l'Energie Atomique and the Centre National de la Recherche Scientifique / Institut National de Physique Nucléaire et de Physique des Particules in France, the Agenzia Spaziale Italiana and the Istituto Nazionale di Fisica Nucleare in Italy, the Ministry of Education, Culture, Sports, Science and Technology (MEXT), High Energy Accelerator Research Organization (KEK) and Japan Aerospace Exploration Agency (JAXA) in Japan, and the K. A. Wallenberg Foundation, the Swedish Research Council and the Swedish National Space Board in Sweden.

Additional support for science analysis during the operations phase is gratefully acknowledged from the Istituto Nazionale di Astrofisica in Italy and the Centre National d'Études Spatiales in France.

This work includes observations obtained with the NASA *Swift* γ-ray burst Explorer. *Swift* is a MIDEX Gamma Ray Burst mission led by NASA with

participation of Italy and the UK.

This research has made use of the Smithsonian/NASA's ADS bibliographic database. This research has made use of the archives and services of the ASI Science Data Center (ASDC), a facility of the Italian Space Agency (ASI Headquarter, Rome, Italy). This research has made use of the NASA/IPAC NED database (JPL CalTech and NASA, USA).

Facilities: *Fermi* LAT, Swift

REFERENCES

Abdo, A. A., Ackermann, M., Ajello, M., et al. 2010a, ApJS, 188, 405
Abdo, A. A., Ackermann, M., Ajello, M., et al. 2010b, ApJ, 722, 520
Abdo, A. A., Ackermann, M., Ajello, M., et al. 2011, ApJ, 733, L26
Ackermann, M. Ajello, M., Albert, A., et al. 2012, ApJS 203 4
Ackermann, M., Ajello, M., Allafort, A., et al. 2011, ApJ, 743, 171
Ackermann, M. Ajello, M., Baldini, L., et al. 2010, ApJ 721 1383
Ade, P. A. R., Aghanim, N., Armitage-Caplan, C. et al. 2014, A&A, 571, A16
Aller, M. C., Kulkarni, V. P., York, D. G., et al. 2012, ApJ, 748, 19
Bagdonaite, J., Jansen, P., Henkel, C., et al. 2013, Science, 339, 46
Barnacka, A., Geller, M. J., Dell'antonio, I. P., & Benbow, W. 2014, ApJ, 788, 139
Barnacka, A., Glicenstein, J.-F., & Moudden, Y. 2011, A&A, 528, L3
Blackburne, J. A., Pooley, D., Rappaport, S., & Schechter, P. L. 2011, ApJ, 729, 34
Blackburne, J. A., Pooley, D., & Rappaport, S. 2006, ApJ, 640, 569
Blandford, R. D., & Narayan, R. 1992, ARA&A, 30, 311
Bisnovatyi-Kogan, G. S., & Tsupko, O. Y. 2010, MNRAS, 404, 1790
Celotti, A., & Ghisellini, G. 2008, MNRAS, 385, 283
Chartas, G., Kochanek, C. S., Dai, X., et al. 2012, ApJ, 757, 137
Chen, B., Dai, X., Kochanek, C. S., et al. 2012, ApJ, 755, 24
Chen, B., Dai, X., Kochanek, C. S., et al. 2011, ApJ, 740, L34
Cheung, C. C., Larsson, S., Scargle, J. D., et al. 2014, ApJ, 782, L14
Ciprini, S. 2010, The Astronomer's Telegram , 2943
Ciprini, S. 2012, The Astronomer's Telegram , 4158
Collmar, W. 2006, ASP Con. Ser. 350, Blazar Variability Workshop II: Entering the GLAST Era, 120
Combi, J. A., & Romero, G. E. 1998, A&AS, 128, 423
Corbet, R., Cheung, C. C., Kerr, M., & Ray, P. S. 2013, in IV Fermi Symposium proc., eConf C121028, (arXiv:1302.5141).
Courbin, F., Lidman, C., Frye, B. L., Magain, P., Broadhurst, T. J., Pahre, M. A., & Djorgovski, S. G. 1998, ApJ, 499, L119
Courbin, F., Meylan, G., Kneib, J.-P., & Lidman, C. 2002, ApJ, 575, 95
Cruz, A., Góra, D., Bernardini, E., 2013, in Proc. of the 33rd ICRC, id 0539, (arXiv:1309.6979, 20)
Dai, X., Mathur, S., Chartas, G., Nair, S., & Garmire, G. P. 2008, AJ, 135, 333
de Rosa, A., Piro, L., Tramacere, A., et al. 2005, A&A, 438, 121
Dermer, C. D., Finke, J. D., Krug, H., Böttcher, M. 2009, ApJ, 692, 32
Dobler, G., & Keeton, C. R. 2006, MNRAS, 365, 1243
Donnarumma, I., De Rosa, A., Vittorini, V. et al. 2011, ApJ, 736, L30
Einstein, A. 1936, Science, 84, 506
Elliot, J. L., & Shapiro, S. L. 1974, ApJ, 192, L3
Fluke, C. J., & Webster, R. L. 1999, MNRAS, 302, 68
Foschini, L., Ghisellini, G., Raiteri, C. M., et al. 2006, A&A, 453, 829
Frye, B. L., Courbin, F., Broadhurst, T. J., Welch, W. J. W., Lidman, C., Magain, P., Pahre, M., & Djorgovski, S. G. 1999, ASP Conf. Series 156, 240
Gehrels, N., Chincarini, G., Giommi, P., et al. 2004, ApJ, 611, 1005
Ghisellini, G., & Tavecchio, F. 2008, MNRAS, 387, 1669
Giommi, P., Polenta, G., Lähteenmäki, A., et al. 2012, A&A, 541, A160
Gregg, M. D., Lacy, M., White, R. L., Glikman, E., Helfand, D., Becker, R. H., & Brotherton, M. S. 2002, ApJ, 564, 133
Grieger, B., Kayser, R., & Schramm, T. 1991, A&A, 252, 508
Hadasch, D., Torres, D. F., Tanaka, T., et al. 2012, ApJ, 749, 54
Hayashida, M., Madejski, G. M., Nalewajko, K., et al. 2012, ApJ, 754, 114
Jauncey, D. L., et al. 1991, Nature, 352, 132
Jin, C., Garrett, M. A., Nair, S., et al. 2003, MNRAS, 340, 1309
Jovanović, P., Zakharov, A. F., Popović, L. Č., & Petrović, T. 2008, MNRAS, 386, 397
Liang, E. W., & Liu, H. T. 2003, MNRAS, 340, 632
Hartman, R. C., et al. 1999, ApJS, 123, 79
Kalberla, P. M. W., Burton, W. B., Hartmann, D., et al. 2005, A&A, 440, 775
Kochanek, C. S., & Narayan, R. 1992, ApJ, 401, 461
Lehár, J., Falco, E. E., Kochanek, C. S., McLeod, B. A., Muñoz, J. A., Impey, C. D., Rix, H.-W., Keeton, C. R., Peng, C. Y. 2000, ApJ, 536, 584
Lidman, C., Courbin, F., Meylan, G., Broadhurst, T., Frye, B., & Welch, W. J. W. 1999, ApJ, 514, L57
Lovell, J. E. J., et al. 1996, ApJ, 472, L5
Lovell, J. E. J., Jauncey, D. L., Reynolds, J. E., Wieringa, M. H., King, E. A., Tzioumis, A. K., McCulloch, P. M., & Edwards, P. G. 1998, ApJ, 508, L51
Marscher, A. P., Jorstad, S. G., Agudo, I., MacDonald, N. R., & Scott, T. L. 2012, in Proceedings of Fermi and Jansky Conference, St Michaels, MD, eConf C1111101, (arXiv:1204.6707)
Marscher, A. P., et al. 2010, ApJ, 710, L126
Martí-Vidal, I., Muller, S., Combes, F., et al. 2013, A&A, 558, AA123
Mathur, S., & Nair, S. 1997, ApJ, 484, 140
Mattox, J. R., Schachter, J., Molnar, L., Hartman, R. C., & Patnaik, A. R. 1997, ApJ, 481, 95
Mattox, J. R., Wagner, S. J., Malkan, M., et al. 1997, ApJ, 476, 692
Mattox, J. R., Bertsch, D. L., Chiang, J., et al. 1996, ApJ, 461, 396
Mosquera, A. M., & Kochanek, C. S. 2011, ApJ, 738, 96
Muller, S., & Guélin, M. 2008, A&A, 491, 739
Muller, S., Beelen, A., Guélin, M., et al. 2011, A&A, 535, A103
Nair, S., Narasimha, D., & Rao, A. P. 1993, ApJ, 407, 46
Nenkova, M., Sirocky, M. M., Nikutta, R., Ivezić, Ž., & Elitzur, M. 2008, ApJ, 685, 160
Nolan, P. L., et al. 2012, ApJS, 199, 31
Oshima, T., Mitsuda, K., Ota, N., Yonehara, A., Hattori, M., Mihara, T., & Sekimoto, Y. 2001, ApJ, 551, 929
Paczynski, B. 1986, ApJ, 304, 1
Perna, R., & Keeton, C. R. 2009, MNRAS, 397, 1084
Pooley, D., Blackburne, J. A., Rappaport, S., Schechter, P. L., & Fong, W.-f. 2006, ApJ, 648, 67
Pramesh Rao, A., & Subrahmanyan, R. 1988, MNRAS, 231, 229
Raiteri, C. M., Villata, M., Aller, M. F., et al. 2011, A&A, 534, A87
Schneider, P., Ehlers, J., & Falco, E. E. 1992, Gravitational Lenses, XIV, 560 pp., Berlin: Springer-Verlag
Sikora, M., Stawarz, Ł., Moderski, R., Nalewajko, K., & Madejski, G. M. 2009, ApJ, 704, 38
Sikora, M., Błażejowski, M., Begelman, M. C., & Moderski, R. 2001, ApJ, 554, 1
Sluse, D., Kishimoto, M., Anguita, T., Wucknitz, O., & Wambsganss, J. 2013, A&A, 553, A53
Sluse, D., Claeskens, J.-F., Hutsemékers, D., & Surdej, J. 2007, A&A, 468, 885
Sokolov, A., & Marscher, A. P. 2005, ApJ, 629, 52
Striani, E., et al. 2009, ATel, 2242, 1
Tanaka, Y. T., Cheung, C. C., Inoue, Y., et al. 2013, ApJ, 777, L18
Torres, D. F., Romero, G. E., Eiroa, E. F., Wambsganss, J., & Pessah, M. E. 2003, MNRAS, 339, 335
van Ommen, T. D., Jones, D. L., Preston, R. A., & Jauncey, D. L. 1995, ApJ, 444, 561
Wambsganss, J. 2001, PASA, 18, 207
Wiklind, T., & Combes, F. 1996, Nature, 379, 139
Wiklind, T., & Combes, F. 1998, ApJ, 500, 129
Wiklind, T., & Combes, F. 2001, ASP Conf. ser., 237, Gravitational Lensing: Recent Progress and Future Goals, 155
Winn, J. N., Kochanek, C. S., McLeod, B. A., et al. 2002, ApJ, 575, 103
Wisotzki, L., Koehler, T., Kayser, R., & Reimers, D. 1993, A&A, 278, L15
Witt, H. J., Mao, S., & Keeton, C. R. 2000, ApJ, 544, 98
Yonehara, A., Mineshige, S., Manmoto, T., et al. 1998, ApJ, 501, L41
Zhang, S., Chen, Y.-p., Collmar, W., Foschini, L., Li, T.-P., Torres, D. F., & Wang, J.-M. 2008b, ApJ, 683, 400
Zimmer, F., Schmidt, R. W., & Wambsganss, J. 2011, MNRAS, 413, 1099